# A Two-Phase Epidemic Driven by Diffusion

Timothy Reluga

*treluga@amath.washington.edu*

Department of Applied Mathematics

University of Washington

Seattle, WA 98195

March, 2004

**Abstract**

In this paper, I present and analyze a model for the spatial dynamics of an epidemic following the point release of an infectious agent. Under conditions where the infectious agent disperses rapidly, relative to the dispersal rate of individuals, the resulting epidemic exhibits two distinct phases: a primary phase in which an epidemic wavefront propagates at constant speed and a secondary phase with a decelerating wavefront. The behavior of the primary phase is similar to standard results for diffusive epidemic models. The secondary phase may be attributed to the environmental persistence of the infectious agent near the release point. Analytic formulas are given for the invasion speeds and asymptotic infection levels. Qualitatively similar results appear to hold in an extended version of the model that incorporates virus shedding and dispersal of individuals.

Keywords: epidemics, reaction–diffusion, spatial dynamics, invasion speed

# 1 Introduction

There has been a recent impetus for the study of spatial epidemiology, following the planned investment of billions of dollars by the United States government in biological weapons defense (Fauci, 2003) and concerns over the potential use of smallpox and other diseases as biological weapons (Henderson, 1999; Breman and Henderson, 2002). In this paper, I study a pedagogical partial differential equation model for a spatial epidemic following the point release of a rapidly dispersing infectious agent, in the hope that it will aid our general understanding of spatially epidemiology.

Spatial models of epidemics and epizootics have existed for at least forty years (Kendall, 1965). One of the first applications of reaction–diffusion theory to spatial epidemiology was an effort by Noble (1974) to describe the spread of plague through Europe in the mid-fourteenth century. Recently, Caraco et al. (2002) have used a reaction–diffusion model to describe the spatial aspects of Lyme disease transmission. Perhaps the most well known and well studied spatial epizootic model is that of Kallen et al. (1985), which describes the spatial dynamics of rabies in fox populations. In its original form, this model is a simplification of Noble's plague model (Noble, 1974). Let $S$ be the concentration of fox susceptible to rabies infection and $I$ be the concentration of rabid fox, i.e., fox infected with rabies. Assuming mass action kinetics and no latency period between infection and symptomatic behavior, the rate at which susceptible fox become infected will be proportional to both the concentration of susceptible fox and the concentration of rabid fox. Mortality will remove rabid fox at a rate proportional to the concentration of rabid fox. Using the assumption that spatial dispersal of rabid fox can be approximated by a diffusion process, Kallen et al. described the dynamics of a rabies epizootic as

$$\dot{S} = -SI \,, \tag{1.1}$$

$$\dot{I} = \quad SI - I + D_I \nabla^2 I \,, \tag{1.2}$$

where $D_I$ is the diffusion rate for rabid fox, the dot represents differentiation with respect to time, and $\nabla^2$ represents a spatial Laplacian operator.

Kallen et al. showed that if the initial concentration of susceptible fox ($S_0$) is greater than the threshold value $\mu/\beta$, then the model described by Eqs. (1.1) and (1.2) possesses traveling wave solutions with asymptotic speed

$$2\sqrt{D_I\,(S_0-1)}\;. \tag{1.3}$$

In the wake of the epidemic wave, the concentration of susceptible fox is reduced to a level ($S_\infty$) that is easily calculated. Murray (2003) presents a contemporary analysis of the this model and its generalizations.

Although more complicated models of disease dispersal have been constructed (Bailey, 1975; Kendall, 1965), many of these models have the same qualitative dynamics: there is a critical threshold for the initial susceptible population below which there is no epidemic wave but above which there exists a traveling wave solution with constant speed and shape. The apparent generality of these results makes it tempting to extrapolate from these models to more complex situations. In some cases, however, this extrapolation may be incomplete. Specifically, important dynamics may occur even after the passage of a primary epidemic wave.

This paper describes a dynamic model of an epidemic following the point-release of an infectious agent under certain limiting assumptions including the rapid dispersal of agent and the absence of virus shedding. Under these assumptions, there exists a critical initial population concentration above which a primary phase epidemic wavefront can be observed to propagate with constant speed. In addition to this primary phase, a secondary epidemic phase can be observed regardless of the initial concentration. This secondary phase, consisting of either a spatially localized transient or a decelerating wave of variable shape, is absent from conventional models though its practical importance may equal that of the primary phase.

The model is described in detail in Section 2. I perform a thorough mathematical analysis in Section 3. Section 4 discusses the robustness of this analysis relative to an extended model incorporating virus-shedding and dispersal of individuals. The contents of Section 3 and 4 are summarized and discussed in Section 5.

# 2 Model Formulation

Let us consider an infectious disease that can be transmitted by both exposure to infectious individuals and exposure to an infectious agent. A natural approach, then, is to extend the classical SIR model (Kermack and McKendrick, 1991) with a new variable ($\hat{A}$) describing the concentration of the infectious agent. In this modified SIR model, henceforth the SIR-A model, susceptible individuals ($\hat{S}$) may become infected by exposure to infectious individuals ($\hat{I}$) at rate $\hat{\beta}_I$ or by exposure to the infectious agent ($\hat{A}$) at rate $\hat{\beta}_A$. Individuals may be classified as removed ($\hat{R}$) if they were resistant due to prior exposure ($\hat{R}_0$) or they were previously infectious and have been quarantined, or have died (collectively represented by the clearance rate $\hat{\mu}$). Mathematically,

$$\frac{d\hat{S}}{d\hat{t}} = -\hat{S}\left(\hat{\beta}_I\hat{I} + \hat{\beta}_A\hat{A}\right) , \tag{2.1}$$

$$\frac{d\hat{I}}{d\hat{t}} = \hat{S}\left(\hat{\beta}_I\hat{I} + \hat{\beta}_A\hat{A}\right) - \hat{\mu}\hat{I} , \tag{2.2}$$

$$\frac{d\hat{R}}{d\hat{t}} = \hat{\mu}\hat{I} , \tag{2.3}$$

with initial conditions

$$\hat{S}(\hat{t}=0) = \hat{S}_0, \quad \hat{I}(\hat{t}=0) = 0, \quad \hat{R}(\hat{t}=0) = \hat{R}_0 . \tag{2.4}$$

As a bookkeeping convenience, I denote dimensional parameters and variables with a hat and reserve hat-less notation for dimensionless parameters and variables.

There are numerous potential descriptions for the dispersal dynamics of the infectious agent $\hat{A}$. I will adopt a simple and conservative approach by neglecting advection (admittedly, a phenomenon of great practical importance), and modeling dispersal as diffusion from a point source. The point release of a finite mass $\hat{A}_0$ of an infectious agent can be represented as a concentration using a delta distribution

$$\hat{A}(\hat{t}=0,\hat{r}) = \hat{A}_0\delta(\hat{r}) , \tag{2.5}$$

where $\hat{r}$ denotes radial distance. Over time, this initial release will diffuse through space, but also decay at some rate ($\hat{\gamma}$) as a result of environmental effects. It is convenient to assume

space is isotropic so that the diffusion process is rotationally symmetric. Under these conditions, the temporal evolution of the agent's concentration may be stated in polar coordinates as

$$\frac{\partial \hat{A}}{\partial \hat{t}} = \hat{D}\left(\frac{\partial^2 \hat{A}}{\partial \hat{r}^2} + \frac{n-1}{\hat{r}}\frac{\partial \hat{A}}{\partial \hat{r}}\right) - \hat{\gamma}\hat{A}\,, \tag{2.6}$$

where $\hat{r}$ is the radial distance from the origin of release, $\hat{D}$ is the diffusion rate, $\hat{\gamma}$ is the rate of decay, and $n$ is the number of dimensions. We will be primarily concerned with the case $n = 2$, where the agent is diffusing in some thin layer across an area, but the mathematics of the problem makes the more general $n$-dimensional approach prudent.

This is perhaps the simplest model available for the dynamics following a point-release of infectious agent. Under one potential extension of this model, the susceptible, infectious, and removed classes should also be allowed to disperse. Another potential extension of this model would be to include "virus shedding", which would allow for the production of infectious agent at some rate proportional to the number of infected individuals. A technical detail that should also be included is removal of infectious agent at a rate proportional to the infection rate. The addition of these effects leads to a system of non-linear reaction–diffusion equations of the form

$$\frac{d\hat{S}}{d\hat{t}} = \hat{D}_S\nabla^2\hat{S} - \hat{S}\left(\hat{\beta}_I\hat{I} + \hat{\beta}_A\hat{A}\right)\,, \tag{2.7}$$

$$\frac{d\hat{I}}{d\hat{t}} = \hat{D}_I\nabla^2\hat{I} + \hat{S}\left(\hat{\beta}_I\hat{I} + \hat{\beta}_A\hat{A}\right) - \hat{\mu}\hat{I}\,, \tag{2.8}$$

$$\frac{d\hat{R}}{d\hat{t}} = \hat{\mu}\hat{I}\,, \tag{2.9}$$

$$\frac{d\hat{A}}{d\hat{t}} = \hat{D}_A\nabla^2\hat{A} - \hat{\eta}\hat{\beta}_A\hat{A}\hat{S} + \hat{\rho}\hat{I} - \hat{\gamma}\hat{A}. \tag{2.10}$$

The relationship between this extended SIR-A model and the regular SIR-A model described by Eqs. (2.1)-(2.6) will be discussed in Section 4.

# 3 Analysis

Our first step in the study of Eqs. (2.1)-(2.6) is to perform a dimensional analysis based on the Buckingham Pi-theorem (Bluman and Anco, 2002). Let

$$S = \hat{S}\hat{\beta}_I/\hat{\mu},\ I = \hat{I}\hat{\beta}_I/\hat{\mu},\ R = \hat{R}\hat{\beta}_I/\hat{\mu},\ A = \hat{A}\hat{\beta}_A/\hat{\mu},\ t = \hat{t}\hat{\mu},\ \text{and}\ r = \hat{r}\sqrt{\frac{\hat{\mu}}{\hat{D}}}\ . \tag{3.1}$$

It follows that the dynamics described by Eqs. (2.1)-(2.6) are equivalent under this change of variables to the dimensionless system

$$\dot{S} = -S(I+A)\ , \tag{3.2}$$

$$\dot{I} = S(I+A) - I\ , \tag{3.3}$$

$$\dot{R} = I\ , \tag{3.4}$$

$$\dot{A} = \left(\frac{\partial^2 A}{\partial r^2} + \frac{n-1}{r}\frac{\partial A}{\partial r}\right) - \gamma A\ , \tag{3.5}$$

with

$$S(t=0,r) = S_0,\ I(t=0,r) = 0,\ R(t=0,r) = R_0,\ \text{and}\ A(t=0,r) = A_0\delta(r)\ , \tag{3.6}$$

where

$$\gamma = \hat{\gamma}/\hat{\mu},\ S_0 = \hat{S}_0\hat{\beta}_I/\hat{\mu},\ R_0 = \hat{R}_0\hat{\beta}_I/\hat{\mu},\ \text{and}\ A_0 = \hat{A}_0\hat{\beta}_A\hat{\mu}^{(n-2)/2}\hat{D}^{-n/2}\ . \tag{3.7}$$

Dimensional analysis illuminates the symmetry relationships among model parameters. Practices that lower the contact rate $\hat{\beta}_I$ between susceptible and infectious individuals will reduce the effective size of the initially susceptible population $S_0$. Effects like faster mortality that increase $\hat{\mu}$ will decrease the effective size of the initial populations $S_0$ and $R_0$.

Before proceeding, we can perform two mathematical simplifications that will ease our work. First, observe that $\dot{S}+\dot{I}+\dot{R} = 0$. It follows that the dynamics of $R$ can be completely described in terms of $S$ and $I$ as

$$R(t) = R_0 + S_0 - S(t) - I(t)\ . \tag{3.8}$$

Second, observe that the dynamics of the infectious agent $A(r,t)$ are decoupled from the other variables. Eq. (3.5) is a linear partial differential equation. For the given initial condition,

the solution of Eq. (3.5) is a normal distribution (see Appendix A). Thus, the model may be reduced to the analysis of a system of two non-linear, non-autonomous ordinary differential equations at various radii $r$ from the point of release:

$$\dot{S} = -S(I+A), \tag{3.9}$$

$$\dot{I} = \ S(I+A) - I, \tag{3.10}$$

$$\text{where} \quad A(t,r) = A_0 \, (4\pi t)^{-n/2} \, e^{-\frac{r^2}{4t} - \gamma t} \ . \tag{3.11}$$

I will now proceed with a mathematical analysis of the SIR-A model described by Eqs. (3.9)-(3.11) using numerical methods, linearization theory, classical asymptotics, and perturbation theory. Readers not interested in the specifics of the mathematical analysis may move directly to Section 5, where these results are summarized and interpreted.

## 3.1 Numerical solutions

The SIR-A model described by Eqs. (3.9)-(3.11) can be integrated numerically using a fourth-order Runge-Kutta-Fehlberg method as long as the peculiarities of the problem are taken into account.

The difficulty in the integration of Eqs. (3.9) and (3.10) is that the forcing, Eq. (3.11), is numerically singular at $t = 0$. A standard remedy is to employ a Taylor series approximation near the singularity. Unfortunately, the Taylor series at $t = 0$ vanishes to all orders in the case of Eq. (3.11). Instead, the singularity can be avoided by starting all integrations at a strictly positive time $t_{min} \approx 10^{-5}$, while keeping the same initial conditions for the susceptible and infectious populations. The error introduced by this approximation was tested by comparison with runs performed at $t_{min} = 10^{-4}$ and $t_{min} = 10^{-6}$. For most of the spatial domain, the use of a small positive starting time does not introduce significant error. However, the singular behavior of Eq. (3.11) makes the SIR-A model stiff for small values of $r$ and $t$, and the use of a finite positive initial time introduces significant error for distances $r \leq 2\sqrt{t_{min}}$. Since our central concerns will be with significantly larger $r$, this is an acceptable compromise, but should be taken into account when studying Figs. 1, 2, and 4.

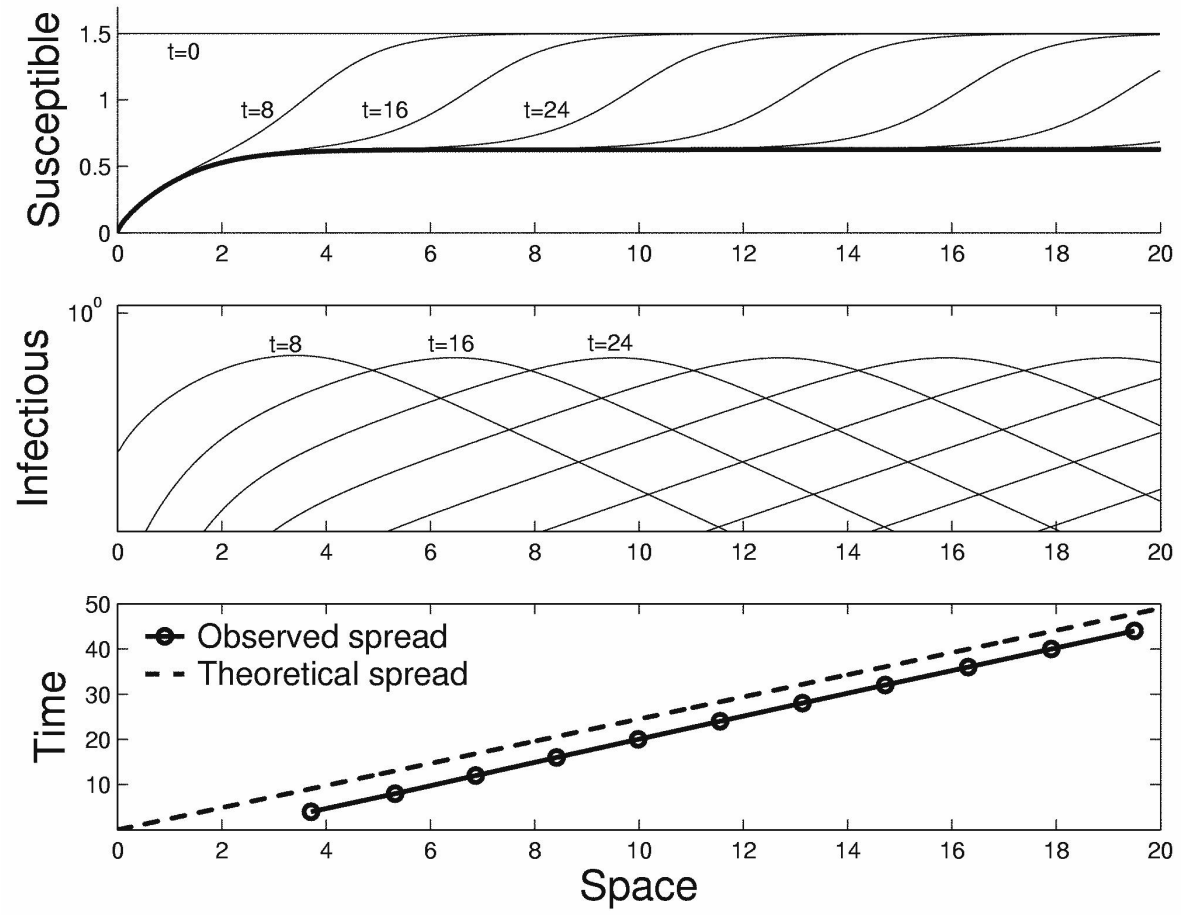


Figure 1 Solution snapshots of the concentrations of susceptible (top) and infectious (middle) individuals every 8.0 time units, with $\gamma = 1$, $S_0 = 1.5$, $A_0 = 4$, and $n = 2$. The lower bound in the top plot corresponds to the $S_\infty$ approximation of Eq. (3.37). The bottom plot shows the position of the primary wave front, calculated using a threshold value of $\delta = 0.1$, and the theoretically position as predicted using the asymptotic speed in Eq. (3.23). The observed speed is 0.397. The theoretically predicted speed is 0.408.

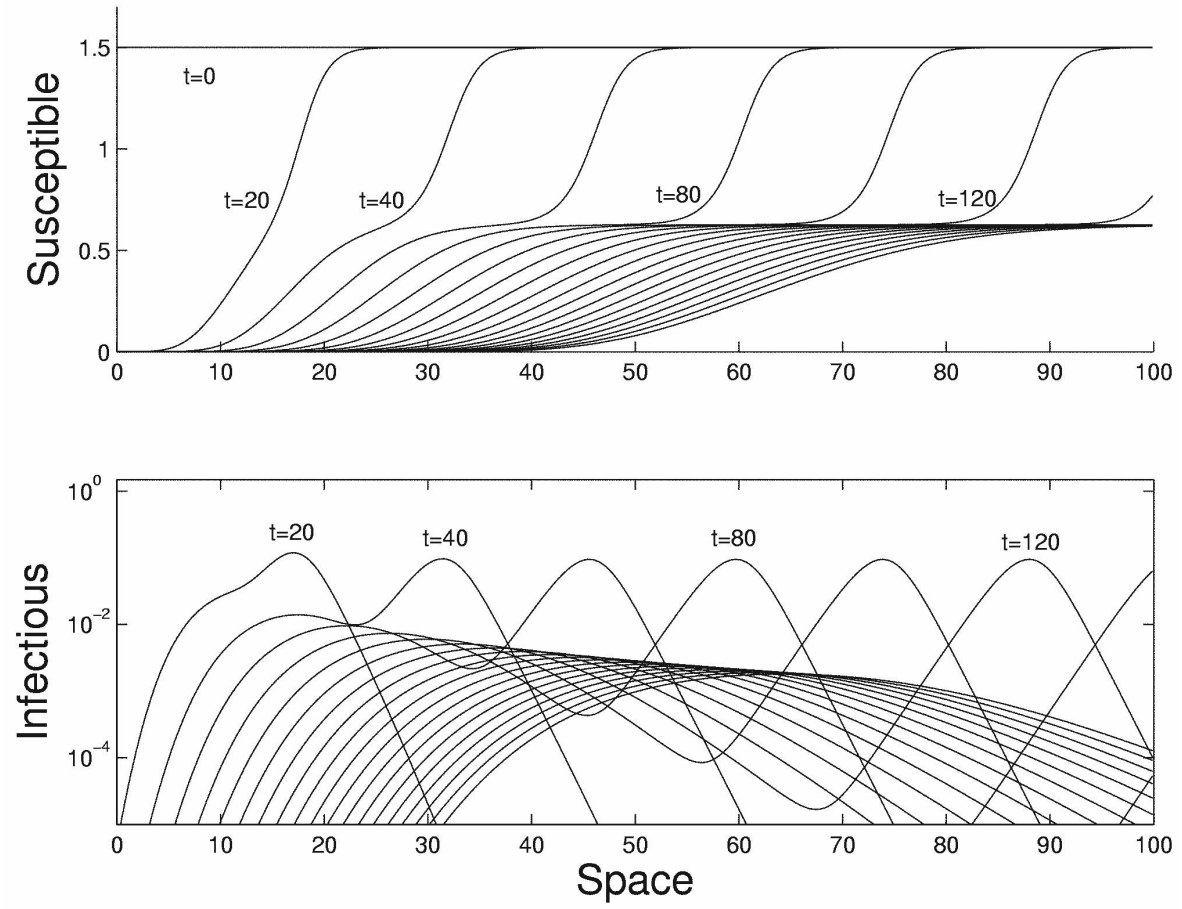


Figure 2 Solution snapshots of the concentration of susceptible (top) and infectious (bottom) individuals in a population in $n = 1$ dimension every 20 time units up to $t = 400$, with $\gamma = 0$, $S_0 = 1.5$, and $A_0 = 4.0$. For large $r$, after the primary wave has passed, the slow secondary wave eventually drives the concentration of susceptible individuals to 0.

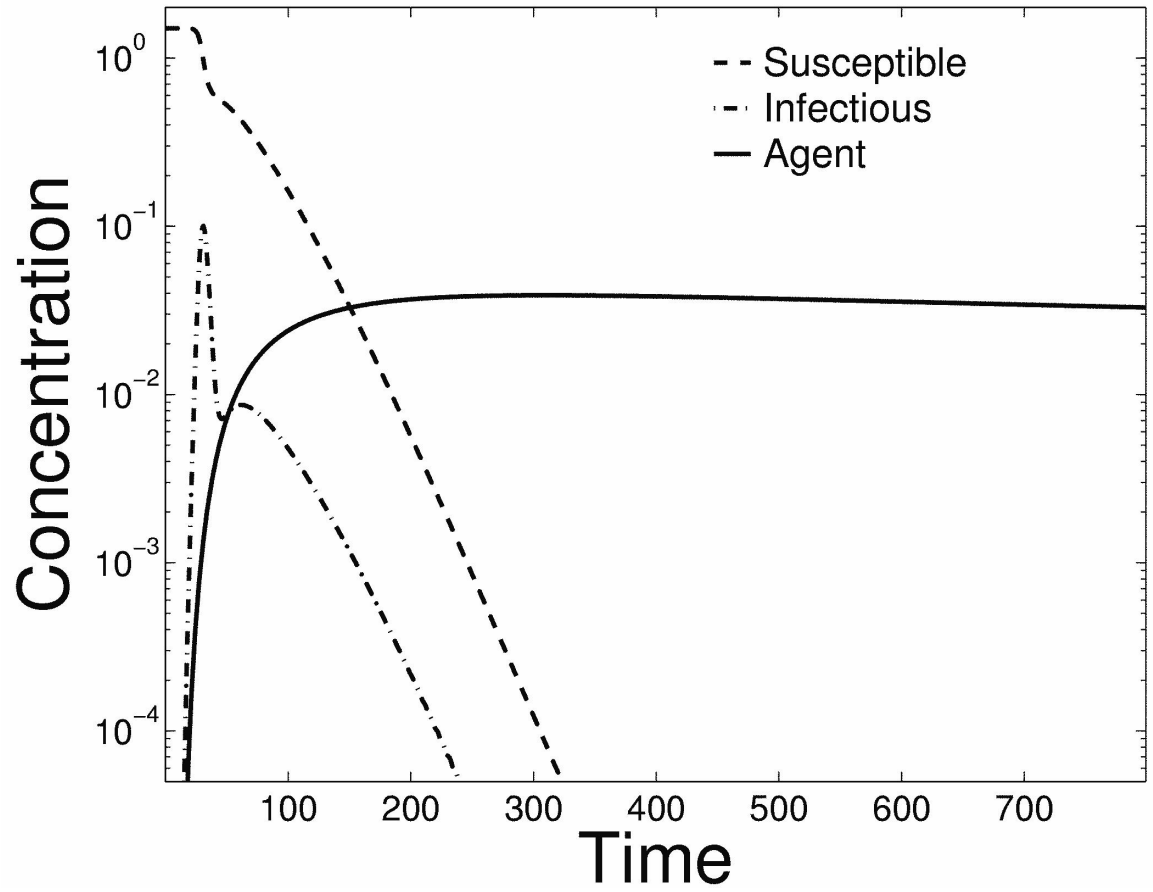


Figure 3 Time series of susceptible individual, infectious individual, and infectious agent concentrations at distance $r = 40$ for parameter values matching those of Fig. 2. Note that the time series for the level of infectious individuals is bimodal, and that both susceptible and infectious concentrations decay exponentially. Though difficult to see, the agent concentration reaches its maximum around $t = 400$ before decaying algebraically.

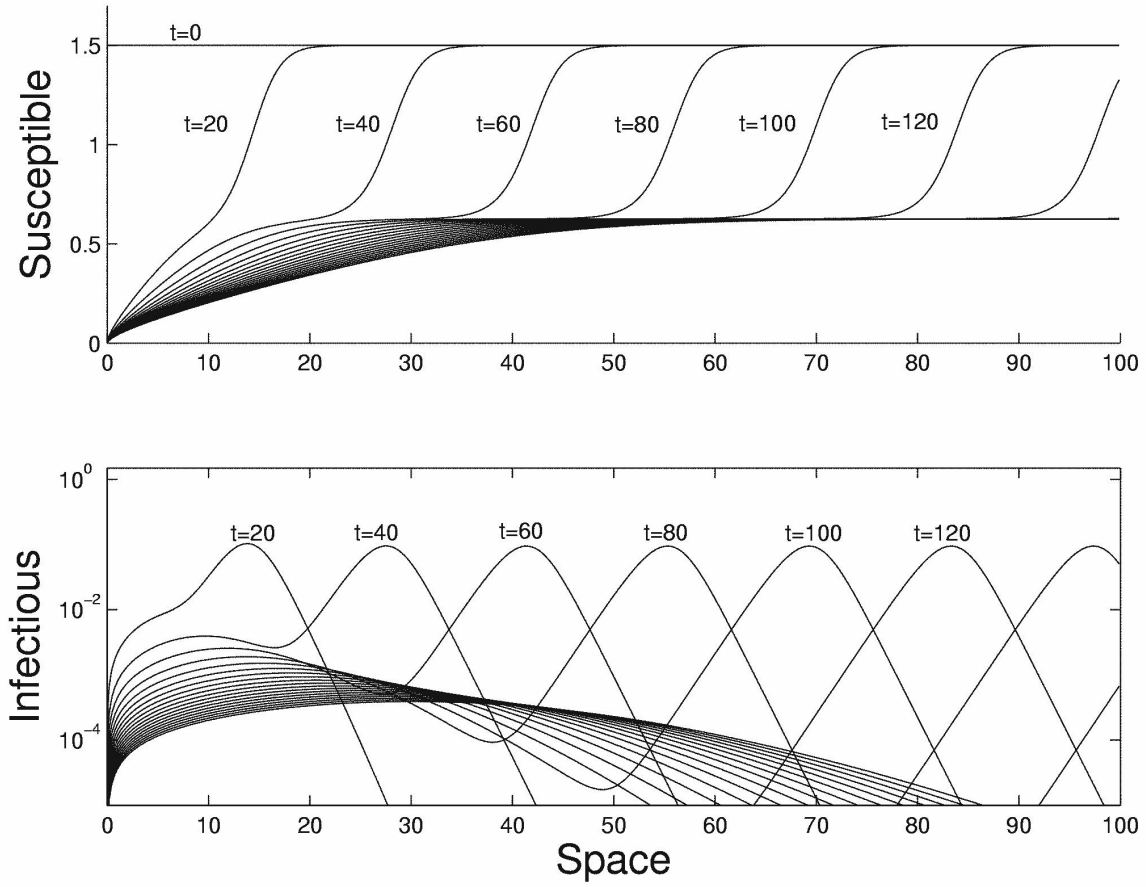


Figure 4 Solution snapshots of the concentration of susceptible (top) and infectious (bottom) individuals in a population in $n = 2$ dimensions every 20 time units up to $t = 400$, with $\gamma = 0$, $S_0 = 1.5$, and $A_0 = 4$. Compared with the one dimensional case (Fig. 2), the secondary phase wavefront has slower advance, but will still eventually drive the susceptible population to 0.

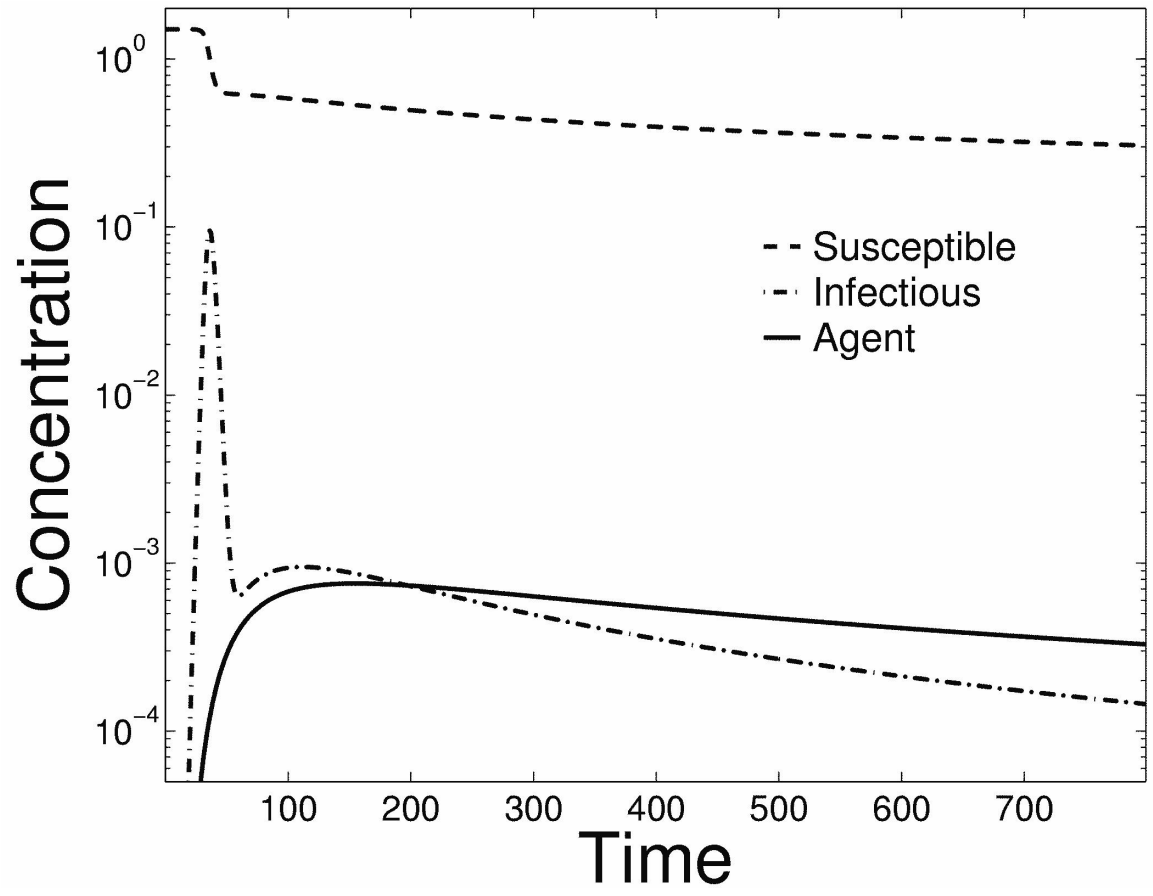


Figure 5 Time series of susceptible individuals, infectious individuals, and infectious agent concentrations at distance $r = 25$ for parameter values matching those of Fig. 4. The concentration of agent ($A$) has a smaller maximum and decays more quickly in two dimensions than in one dimension (see Fig. 3 for comparison).

Some examples of the dynamics of the SIR-A model can be seen in Figs. 1-5. Figures 3 and 5 show the time series of infection when observed at a single point in space for the one and two dimensional models, respectively. Both show a bimodal behavior in the concentration of infectious individuals. Figures 1, 2, and 4 show three cases of the SIR-A model's spatial dynamics. In all three examples, there is a clear primary phase consisting of a wave of infection that appears to travel at a constant speed. In Figures 2 and 4, there also appears to be a secondary phase, with a significantly slower spread rate.

Numerical solutions of the extended SIR-A model on a finite domain with Neumann boundary conditions were obtained in one dimension using Matlab's built-in routine for solving systems of parabolic partial differential equations. The domain was enlarged to minimize boundary-effects in the observed region, and the finite initial time procedure described above was used to avoid singularities at small time. Figure 6 shows snapshots of an example solution to the dimensionless form the extended SIR-A model, Eqs. (4.1)-(4.4).

Numerical methods do no provide generalizable results. Fortunately, significant insight into the general dynamics of the SIR-A model can be gained through algebraic analysis. As I shall show, the two phases of behavior suggested by Figs. 1-5 do exist, and reflect a combination of the well known threshold behavior of the SIR model and the dispersal of a persistent infectious agent. First, however, a little groundwork on waves must be laid.

## 3.2 non-Autonomous Kinematic Waves

A standard problem in spatial models is the determination of the minimum speed $c^*$ for which a model admits traveling wave solutions of the form $F(x - c^*t)$, where $F$ is a vector-valued function and $c^*$ is a positive scalar. However, the SIR-A model described by Eqs. (3.9)-(3.11) does not possess traveling wave solutions in the strict mathematical sense because of the transient forcing term. Despite this, numerical simulations like Fig. 1 suggest that Eqs. (3.9)-(3.11) do possess wave fronts that behave locally like traveling waves when $S_0 > 1$. There is an extensive literature on traveling waves in reaction–diffusion equations (Murray, 2003; Grindrod, 1996), but less work addressing forced systems similar to the SIR-A model.

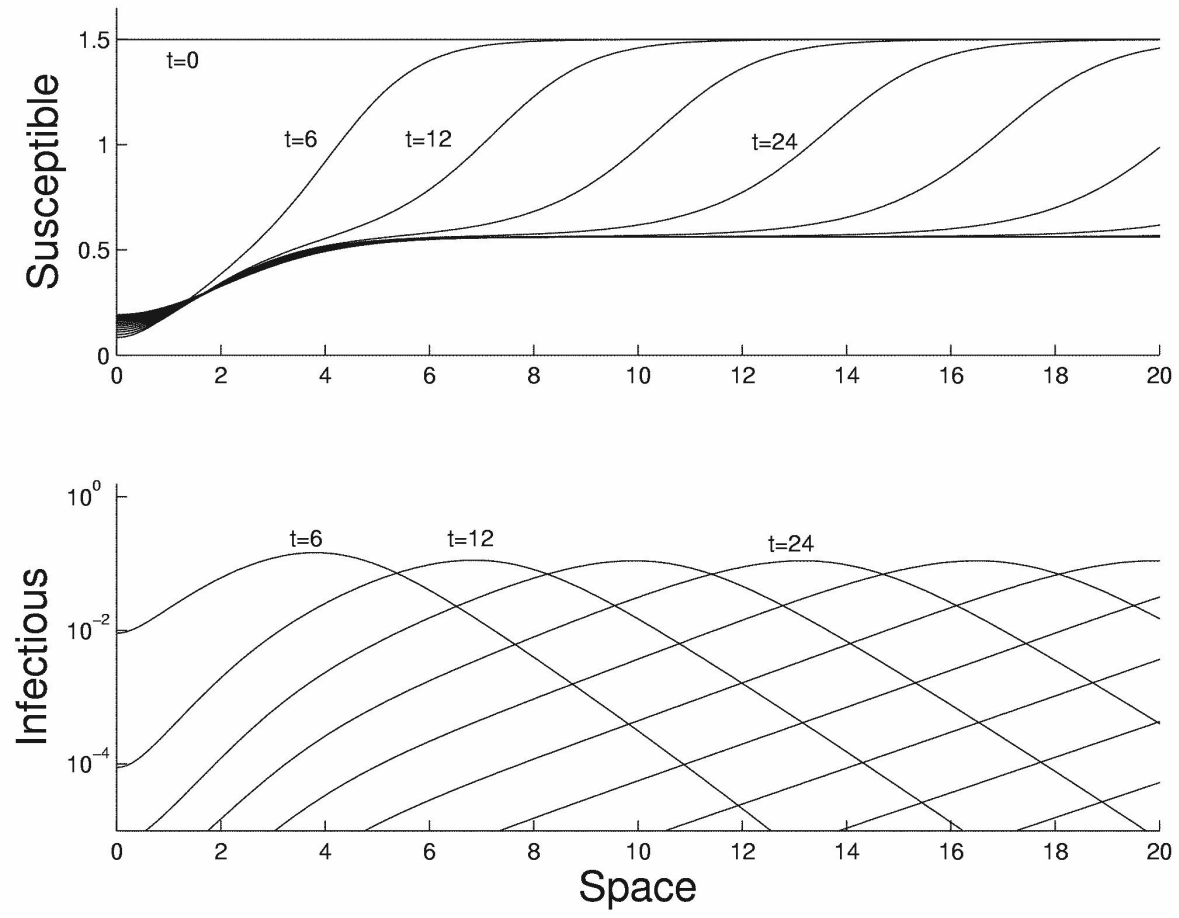


Figure 6 Solution snapshots from the extended SIR-A model of the concentrations of susceptible (top) and infectious (bottom) individuals every 6.0 time units, with $D_S = D_I = 0.01$, $\eta = 0.01$, $\rho = 0.05$, $\gamma = 1$, $S_0 = 1.5$, and $A_0 = 4$. Note that the secondary phase is present with finite size near the point of release but is slowly eroded by the dispersal of susceptible individuals.

One exception appears to be work of Cook (see Murray, 2003, chap. 13). Because of the novelty of the problem, it is prudent to define some basic terms.

Let the position $p$ of a wavefront at time $t$ be defined as the farthest position for which the norm of the concentration levels with respect to given reference concentrations is less than some threshold ($\delta$). Mathematically, we may define the position as the function

$$p(\delta,t) = \sup\left\{r > 0 : [S_0 - S(t,r)]^2 + I^2(t,r) < \delta^2\right\}\ , \tag{3.12}$$

where $I(t,r)$ and $S(t,r)$ are concentrations of infectious and susceptible individuals at time $t$ and radius $r$. The position function $p(\delta,t)$ may be discontinuous or even undefined for some values of $\delta$ and $t$, but will never be multi-valued.

A wave has asymptotic speed $c^*(\delta)$ if for every $\varepsilon > 0$, there exists $T > 0$ so that for every $t > T$,

$$[c^*(\delta) - \varepsilon]t < p(\delta,t) < [c^*(\delta) + \varepsilon]t. \tag{3.13}$$

In addition, we can say a wave front is traveling wave-like if for some non-vanishing range of threshold values $\mathcal{D} \ni \delta$, the asymptotic speed $c^*(\delta) = c^*$, independent of $\delta$.

Our definition of asymptotic spread rate contains an important difference from the conventional definition used in reaction–diffusion theory. Specifically, the above definition makes no attempt to generalize the asymptotic speed $c^*$ over different initial conditions. In contrast, the asymptotic spread rate in reaction–diffusion equations is minimized over all initial conditions to obtain a realized asymptotic spread rate. This procedure is inappropriate for the $SIR-A$ model, where we are concerned with a specific scenario of initial conditions.

## 3.3 Epidemic fronts for $S_0 > 1$

Having framed the problem with the above definitions, we can now ask under what conditions the SIR-A model has solutions with traveling wave-like behavior. The case of small $\delta$ is of immediate interest because it describes the initial dynamics of infection. If $\delta$ is small, then $S(t,r) \approx S_0$ and $I(t,r) \approx 0$. We can approximate the infection dynamics of Eq. (3.10) as

$$\dot{I} - (S_0 - 1)I \approx S_0 A. \tag{3.14}$$

Eq. (3.14), henceforth referred to as the linearized SIR-A model, is of fundamental importance in the solution of the invasion speed problem for the SIR-A model. Since $I$ grows faster in the linearized SIR-A model than it does in the full SIR-A model, it is evident that the asymptotic rate of spread of the linearized SIR-A model must provide an upper bound on the actual asymptotic rate of spread. Additionally, I will argue that the rate of spread in the linearized SIR-A model actually converges to the asymptotic rate of spread in the full model for sufficiently small $\delta$, although there are some important caveats on this result.

To calculate the spread rate of the linearized SIR-A model, we must solve Eq. (3.14). Using integrating factors or a Green function,

$$I(t,r) = S_0 e^{(S_0-1)t} \int_0^t A(t=\tau,r) e^{-(S_0-1)\tau} d\tau \tag{3.15}$$

$$= S_0 A_0 e^{(S_0-1)t} \int_0^t (4\pi\tau)^{-n/2} e^{-\frac{r^2}{4\tau}-(\gamma-1+S_0)\tau} d\tau\,. \tag{3.16}$$

I am unaware of a closed-form representation for this integral, though several special cases are discussed in Appendix B. Instead, Eq. (3.16) is analyzed asymptotically. For large time $t$, there are two cases of interest: $S_0 < 1$ and $S_0 > 1$. If $S_0 < 1$, the epidemic will not be self-sustaining and most infection will be caused by environmental exposure to the originating agent. If, on the other hand, $S_0 > 1$, the concentration of infectious individuals will initially exhibit exponential growth. In this latter case, the exponential term of the integrand has a local maximum at

$$\tau_0 = \frac{r}{2\sqrt{\gamma+S_0-1}}. \tag{3.17}$$

This suggests the use of the Laplace method (Erdelyi, 1956). For sufficiently large $t$, the exponent may be expanded in a Taylor series about $\tau_0$. Discarding all terms of cubic and higher order, we find the following asymptotically valid approximation: as

$$r\sqrt{\gamma+S_0-1} \to \infty, \tag{3.18}$$

$$I(t,r) \sim S_0 A_0 e^{(S_0-1)t} \int_0^\infty (4\pi\tau)^{-n/2} \exp\left[-r\sqrt{\gamma+S_0-1} - \frac{2}{r}(\gamma+S_0-1)^{3/2}(\tau-\tau_0)^2\right] d\tau\,, \tag{3.19}$$

where the contribution of the integrand from $t$ to $\infty$ is exponentially small. After integrating,

$$I(t,r) \sim \frac{1}{2} A_0 S_0 \left(\gamma + S_0 - 1\right)^{\frac{n-3}{4}} (2\pi)^{\frac{1-n}{2}} \exp\left[(S_0-1)t - r\sqrt{\gamma + S_0 - 1} + \frac{1-n}{2}\ln r\right] . \quad (3.20)$$

On inspection of this asymptotic approximation, we observe that all of the spatial and temporal dependence occurs in the exponential term. Collectively, the exponent

$$\theta(t,r) = (S_0-1)t - r\sqrt{\gamma + S_0 - 1} + \frac{1-n}{2}\ln r \quad (3.21)$$

is called the phase function (Acheson, 1990) of a wave and can be used to calculate several useful quantities. Of specific interest here, the asymptotic speed of a wave can be calculated as

$$c^* = \lim_{t,r\to\infty} -\frac{\partial\theta}{\partial t} \Big/ \frac{\partial\theta}{\partial r} \quad (3.22)$$

$$= \frac{S_0 - 1}{\sqrt{\gamma + S_0 - 1}}. \quad (3.23)$$

Using Eq. (3.20), it can be shown that the speed calculated in Eq. (3.23) satisfies the condition of Eq. (3.13). Thus, the linearized SIR-A model has a constant speed, that depends on the initial concentration of susceptible individuals and the rate of decay of the dispersing agent, but is independent of the amount of agent released.

As observed above, Eq. (3.23) must provide an upper bound on the asymptotic invasion speed of the SIR-A model for compactly supported initial conditions. Demonstrating that the asymptotic speed of the SIR-A model converges to Eq. (3.23) is more difficult but a heuristic argument may be present as follows. The asymptotic approximation in Eq. (3.20) relies on a large-time expansion. However, the linearization, Eq. (3.14), fails for large time. If we carefully disentangle this apparent contradiction, we find that the asymptotic solution of the linearized model fails to approximate the full SIR-A model unless $A_0$ is sufficiently small. But, given small $A_0$, the asymptotic speed of the linearized model is independent of $A_0$ and the asymptotic speed of the full SIR-A model will converge to that of Eq. (3.23) as $A_0 \to 0$. On the other hand, a larger initial release of infectious agent will not reduce the invasion speed, so Eq. 32 must also provide a lower bound on the asymptotic speed. Thus, if Eq. (3.23) is correct in the limit as $A_0 \to 0$, then it must also be correct for all $A_0 > 0$.

This argument rests on treacherous biological ground, however. Every population has a discrete, finite number of individuals. Thus, the continuum-of-population-sizes postulate that allows us to take a limit as $A_0 \to 0$ can not be solidly justified. We can only rigorously justify Eq. (3.23) as an upper bound. A stochastic, individual-based model equivalent to the SIR-A model will probably generate invasions that are slower than $c^*$ (Snyder, 2003), and, in the cases of $\gamma > 0$, these invasions will completely stall on timescales of $(\ln A_0)/\gamma$ because of finite population-size effects leading to extinction of the infectious agent. The lattice effects that arise when the continuum-of-population-sizes postulate fails are a recurrent issue in theoretical ecology. Lattice effects may be important in the description of the dynamics of well-mixed models (Henson et al., 2001), and have received specific attention in invasion theory recently (Clark et al., 2001). Further exposition is beyond the scope of this paper, but $c^*$ also has importance as a lower bound on invasion speed in the extended $SIR-A$ model. This will be discussed in more detail in Section 4.

## 3.4 Asymptotic susceptibility level

The analysis of Section 3.3 describes the initial dynamics of the SIR-A model near the primary invasion front for small time and $S_0 > 1$, but is incorrect for large time ($t$) and subcritical initial populations ($S_0 < 1$). What then is the asymptotic behavior of the SIR-A model? The primary results of this section are formulas for the asymptotic concentration of susceptible individuals ($S_\infty$) and total number of individuals removed from the susceptible class of the course of the epidemic ($M$). These formulas will be obtained using a matched asymptotic expansion.

For the moment, assume the infectious agent has a very short environmental half-life ( $\gamma \gg 1$ ). Initially, the agent must be the only source of infection, but for large time the concentration of agent will be insignificant. This suggests that the local dynamics can be decomposed into two time-scales: an inner boundary layer where the concentration of agent ($A$) dominates the concentration of infectious individuals ($I$), and an outer limit where the concentration of agent is negligible relative to the more slowly decaying concentration of in-

fectious individuals. As such, the problem can be solved using the method of multiple scales (Kevorkian and Cole, 1996). By approximating the dynamics on an inner and outer time scale and matching the solutions in the middle, we may obtain a reasonable approximation to the true solution.

From the functional form of $A(t,r)$, Eq. (3.11), we expect the boundary layer to have thickness on the order of $t \sim r/\sqrt{4\gamma}$ (see Appendix A). This is the approximate time at which $A$ obtains a maximum. In the inner limit, where $t \ll r/\sqrt{4\gamma}$, $I$ is negligible with respect to $A$ and $S$ so that

$$\dot{S} \approx -SA\,, \tag{3.24}$$

$$\dot{I} \approx SA\,. \tag{3.25}$$

This yields an inner solution

$$S_{\text{inner}} = S_0 \exp\left[-\int_0^t A(t=\tau,r)d\tau\right]\,, \tag{3.26}$$

$$I_{\text{inner}} = S_0 - S_{\text{inner}}(t)\,. \tag{3.27}$$

In the outer limit, $A$ has decayed to insignificant levels, so that

$$\dot{S} \approx -SI\,, \tag{3.28}$$

$$\dot{I} \approx SI - I\,. \tag{3.29}$$

These differential equations for the outer solution describe a standard SIR model (Murray, 2003), with first integral

$$H = I_{\text{outer}} + S_{\text{outer}} - \ln S_{\text{outer}}, \tag{3.30}$$

where $H$ is a constant determined by the initial conditions. Eqs. (3.28) and (3.29) do not have a simple closed-form solution but we can calculate the asymptotic limits $(S_\infty, I_\infty)$ using a special function:

$$\lim_{t\to\infty} S_{\text{outer}}(t) \equiv S_\infty = -W_0\left(-S_1 e^{-S_1-I_1}\right)\,, \tag{3.31}$$

$$\lim_{t\to\infty} I_{\text{outer}}(t) \equiv I_\infty = 0\,, \tag{3.32}$$

where $(S_1, I_1)$ is the state of the system at any time for which the outer solution matches the inner solution and $W_0()$ is the principle branch of the Lambert $W$ function (Abramowitz and Stegun, 1972; Corless et al., 1996). The Lambert $W$ function is an inverse function closely related to the natural logarithm in both definition and behavior. While the principle branch of the natural log is defined to satisfy

$$e^{\ln x} = x \,, \tag{3.33}$$

the Lambert $W$ function's principle branch is defined to satisfy

$$W_0(x)e^{W_0(x)} = x \,. \tag{3.34}$$

To match the outer solution to the inner solution, we integrate the inner solution to infinity so that

$$S_1 = \lim_{t\to\infty} S_{\text{inner}}(t) \,, \tag{3.35}$$

$$I_1 = \lim_{t\to\infty} I_{\text{inner}}(t) \,. \tag{3.36}$$

Noting that the inner solution satisfies $S_1 + I_1 = S_0$,

$$S_\infty(r\,;\,\gamma, S_0, A_0) \approx -W_0\left(-S_0 e^{-So-\int_0^\infty A(t=\tau,r;\,\gamma,A_0)d\tau}\right) \,, \tag{3.37}$$

The integral in Eq. (3.37) has a closed-form solution in terms of modified Bessel functions (see Appendix B), and can be calculated using many standard software packages. We have placed no assumptions on $S_0$ up to this point. The $S_\infty$ approximation is valid for both $S_0 < 1$ and $S_0 > 1$. Although derived for short half-lives ($\gamma \gg 1$), Eq. (3.37) is surprisingly accurate, even for long half-lives ($\gamma \sim 1$) as is suggested by Fig. 1

Using Eq. (3.37), we can estimate the asymptotic concentration of removed individuals:

$$R_\infty \approx S_0 - S_\infty\left(r\,;\,\gamma, S_0, A_0\right) \,. \tag{3.38}$$

When the $S_\infty$ approximation is valid for all $r$, the total level of removal in the population ($M$) can be calculated by integrating over the spatial domain:

$$M = C_n \int_0^\infty \left[S_0 - S_\infty(r\,;\,\gamma, S_0, A_0)\right] n r^{n-1} dr \,, \tag{3.39}$$

where $C_n$ is a constant that only depends on the number of dimensions $n$. The integral in Eq. (3.39) will be divergent unless $S_0 < 1$ and $\gamma > 0$. To see how $\gamma$ relates to the total removal level, observe that for the special case of two dimensions ($n = 2$),

$$\int_0^\infty A(t = \tau, r;\, \gamma, A_0) d\tau = \frac{A_0}{2\pi} K_0\left(r\sqrt{\gamma}\right) , \tag{3.40}$$

where $K_0(x)$ is a modified Bessel function (see Appendix B), so that

$$M = C_2 \int_0^\infty \left[S_0 - S_\infty(r\sqrt{\gamma};\, S_0, A_0)\right] r dr . \tag{3.41}$$

In this form, the parameters $r$ and $\gamma$ are coupled. Under the change of variables $v = r\sqrt{\gamma}$,

$$M = \frac{C_2}{\gamma} \int_0^\infty \left[S_0 - S_\infty(v;\, S_0, A_0)\right] v dv . \tag{3.42}$$

Returning to dimensional variables,

$$\hat{M} = C_2 \frac{\hat{\beta}_I}{\hat{\mu}\hat{\gamma}} \int_0^\infty \left[\hat{S}_0 - \hat{S}_\infty\left(v;\, \frac{\hat{S}_0\hat{\beta}_I}{\hat{\mu}}, \frac{\hat{A}_0\hat{\beta}_A}{\hat{D}}\right)\right] v dv . \tag{3.43}$$

The integrand is now independent of $\hat{\gamma}$, though not of the other parameters. so, when $S_0 = \hat{S}_0\hat{\beta}_I/\hat{\mu} < 1$, and $\hat{\gamma} > 0$, the total number of individuals who become infected over the course of the epidemic is inversely proportional to the rate of environmental decay, $\hat{\gamma}$, of the infectious agent.

## 3.5 Pandemic conditions

Section 3.4 suggests that the total infection level becomes infinite at $\gamma = 0$. But this is precisely the case where our approximation of $S_\infty$ should fail, so let us examine the case of $\gamma = 0$ with a little more scrutiny.

Let $\overline{S}(t)$ satisfy

$$\frac{d\overline{S}}{dt} = -\overline{S}A(t), \quad \text{and} \quad \overline{S}(0) = S_0 . \tag{3.44}$$

Then, from comparison to Eq. (3.9), we see that for every positive time,

$$\frac{dS}{dt} < \frac{d\overline{S}}{dt} < 0 . \tag{3.45}$$

Both $\overline{S}(t)$ and $S(t)$ must be monotonically decreasing functions. Since both $\overline{S}(t)$ and $S(t)$ have the same initial condition and are sufficiently smooth, then, for any $t > 0$,

$$0 < S(t) < \overline{S}(t) < S_0 \,, \tag{3.46}$$

$$0 \leq S_\infty \leq \overline{S}_\infty < S_0 \,, \tag{3.47}$$

$$\text{where} \quad \overline{S}_\infty \equiv \lim_{t\to\infty} \overline{S}(t) \quad \text{and} \quad S_\infty \equiv \lim_{t\to\infty} S(t). \tag{3.48}$$

We can be more specific, however, since we can solve for $\overline{S}(t)$ in closed form.

$$\overline{S}(t) = S_0 \exp\left[ -\int_0^t A_0 \,(4\pi t)^{-\frac{n}{2}}\, e^{-r^2/4t - \gamma t} dt \right] \,. \tag{3.49}$$

It can be shown (see Appendix B) that if $\gamma = 0$ and $n \leq 2$, the integral in Eq. (3.49) is divergent and hence, $\overline{S}_\infty = 0$. By the squeeze theorem, we conclude that $S_\infty = 0$ in this case. Thus, everybody must become infected in the one or two dimensional versions of the SIR-A model if $\gamma = 0$ ( see Figs. 3 and 5 ). If $\gamma > 0$ or $n > 2$, it is more difficult to draw conclusions about the asymptotic behavior of $S$, since $\overline{S}_\infty > 0$ (see Appendix B). Numerical results suggest that $S_\infty > 0$ in these cases.

## 3.6 Secondary fronts

For the pandemic situation of Section 3.5, where $S_0 < 1$, $\gamma = 0$, and $n = 1$ or $n = 2$, the system is not excitable in the sense of possessing linear wave with asymptotic speed $c^* > 0$. However, the susceptible population concentration still approaches 0 everywhere in the spatial domain. A quasi-steady-state perturbation argument (Segal and Slemrod, 1989) can be employed to determine the nature of the wave in this case.

According to Eq. (3.11), when $\gamma = 0$, $A$ decays algebraically while $I$ decays exponentially. For long time, when $S$ is small, $I$ may be expected to satisfy the quasi-equilibrium condition $\dot{I} = 0$. Thus,

$$I \approx \frac{SA}{1-S} \,. \tag{3.50}$$

By substitution into Eq. (3.9),

$$\frac{\dot{S}}{S} = \frac{A}{S-1} \,. \tag{3.51}$$

This ordinary differential equation is separable, leading to the implicit solution

$$Se^{-S} = \exp\left[-\int^{t} A(\tau, r;\, n, A_0)d\tau\right] . \tag{3.52}$$

Using Lambert's $W$ function to solve for $S$, we conclude that for sufficiently large $t$,

$$S(t) = -W_0\left(-e^{-\int^t A(\tau,r;\, n,A_0)d\tau}\right) . \tag{3.53}$$

By inspection, we see that wavefronts have phase function

$$\theta(t,r) = \int^{t} A(\tau, r;\, n, A_0)d\tau\, . \tag{3.54}$$

Application of Eq. (3.22) can be used to show that the asymptotic speed of the secondary phase vanishes. However, the rate of spread is more easily understood in terms of the phase function's asymptotic behavior. By plotting the contours of the phase function, we can gain some understanding of the position of a specific phase at a specific time. The asymptotic shape of the phase function's contours describes how the rate of spread is changing.

If $n > 2$, the phase function collapses (see Appendix B). For large $t$, the phase is independent of time,

$$\lim_{t\to\infty} \theta(t,r) \propto r^{2-n}\Gamma\left(\frac{n}{2}-1\right) + C\, , \tag{3.55}$$

implying that the wave becomes stationary. In 1 and 2 dimensions, however, the phase function does not become time independent. In one dimension ( $n = 1$ ), Eq. (3.54) can be reduced to ( see Appendix B )

$$\theta(t,r) = \sqrt{\frac{t}{\pi}}e^{-\frac{r^2}{4t}} - \frac{r}{2}\,\mathrm{erfc}\left(\frac{r}{2\sqrt{t}}\right) , \tag{3.56}$$

where $\mathrm{erfc}(x)$ is the complementary error function (Abramowitz and Stegun, 1972). For large $r$ and $t$,

$$\theta(t,r) \propto \frac{t\ln t}{r^2} . \tag{3.57}$$

In two dimensions ($n = 2$), Eq. (3.54) reduces to

$$\theta(t,r) = \frac{1}{4\pi}\mathrm{E}_1\left(\frac{r^2}{4t}\right) , \tag{3.58}$$

where $\mathrm{E}_1(x)$ denotes the type 1 exponential integral (see Appendix B).

As seen in Figs. 7 and 8, the phase functions in one and two dimensions, Eqs. (3.56) and (3.58) respectively, describe decelerating wave fronts. The radial positions $r$ grow in time at sub-linear rates when the phase is held constant. The fanning out of the constant phase contours corresponds to changes in the wavefront's shape. As the secondary wavefront evolves, it becomes flatter. If the wavefront becomes steeper, the contours will pinch together instead. Since area is proportional to radius squared, the two dimensional phase function can be conveniently reinterpreted as allowing the area occupied by the wavefront to grow linearly in time.

# 4 The extended SIR-A model

The SIR-A model provides a simple mathematical description of epidemic dynamics following the point release of an infectious agent but at the cost of some very restrictive assumptions. As discussed in Section 2, Eqs. (2.7)-(2.10) describe an extended SIR-A model that incorporates dispersal of all the active components, virus shedding, and a non-linear mass-balance term describing consumption of agent. After using a dimensional analysis procedure similar to that of Section 3, it is sufficient to consider the dimensionless extended SIR-A model

$$\frac{dS}{dt} = D_S \nabla^2 S - S(I+A), \tag{4.1}$$

$$\frac{dI}{dt} = D_I \nabla^2 I + S(I+A) - I, \tag{4.2}$$

$$\frac{dR}{dt} = I, \tag{4.3}$$

$$\frac{dA}{dt} = \nabla^2 A - \eta A S + \rho I - \gamma A. \tag{4.4}$$

It is difficult to obtain closed form solutions for Eqs. (4.1)-(4.4) because of the non-linearity and the coupling terms. Numerical solutions show that when $D_I, D_S, \eta,$ and $\rho$ are small, dynamics are similar to those of the simplified model (see Figure 6). Specifically, we can still observe the primary phase epidemic wave and the secondary phase mortality effect concentrated near the release site.

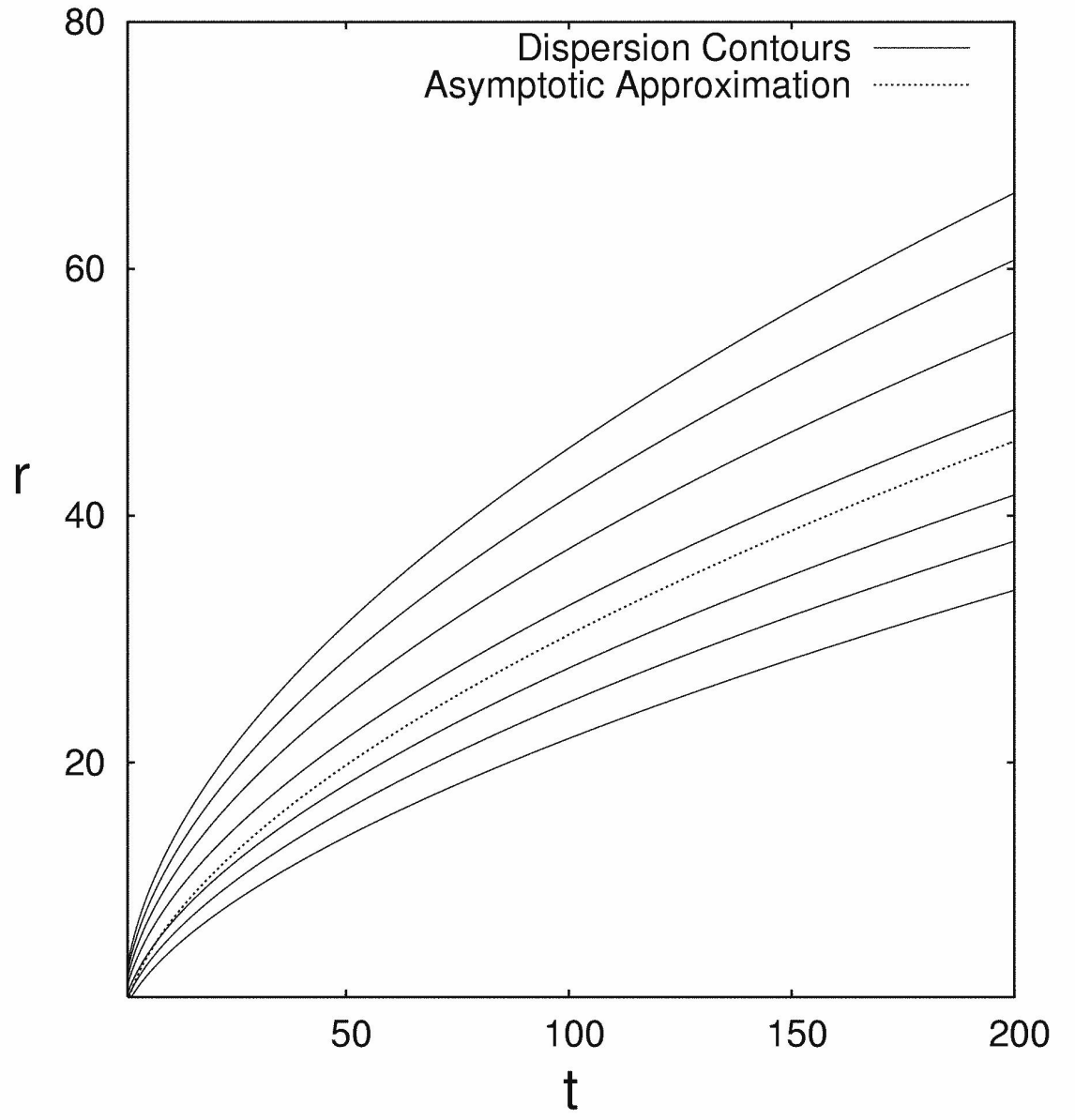


Figure 7 Phase function contours for the secondary wavefront in $n = 1$ dimension, as described in Eq. (3.56) for immortal agent ($\gamma = 0$), along with an asymptotic approximation based on Eq. (3.57).

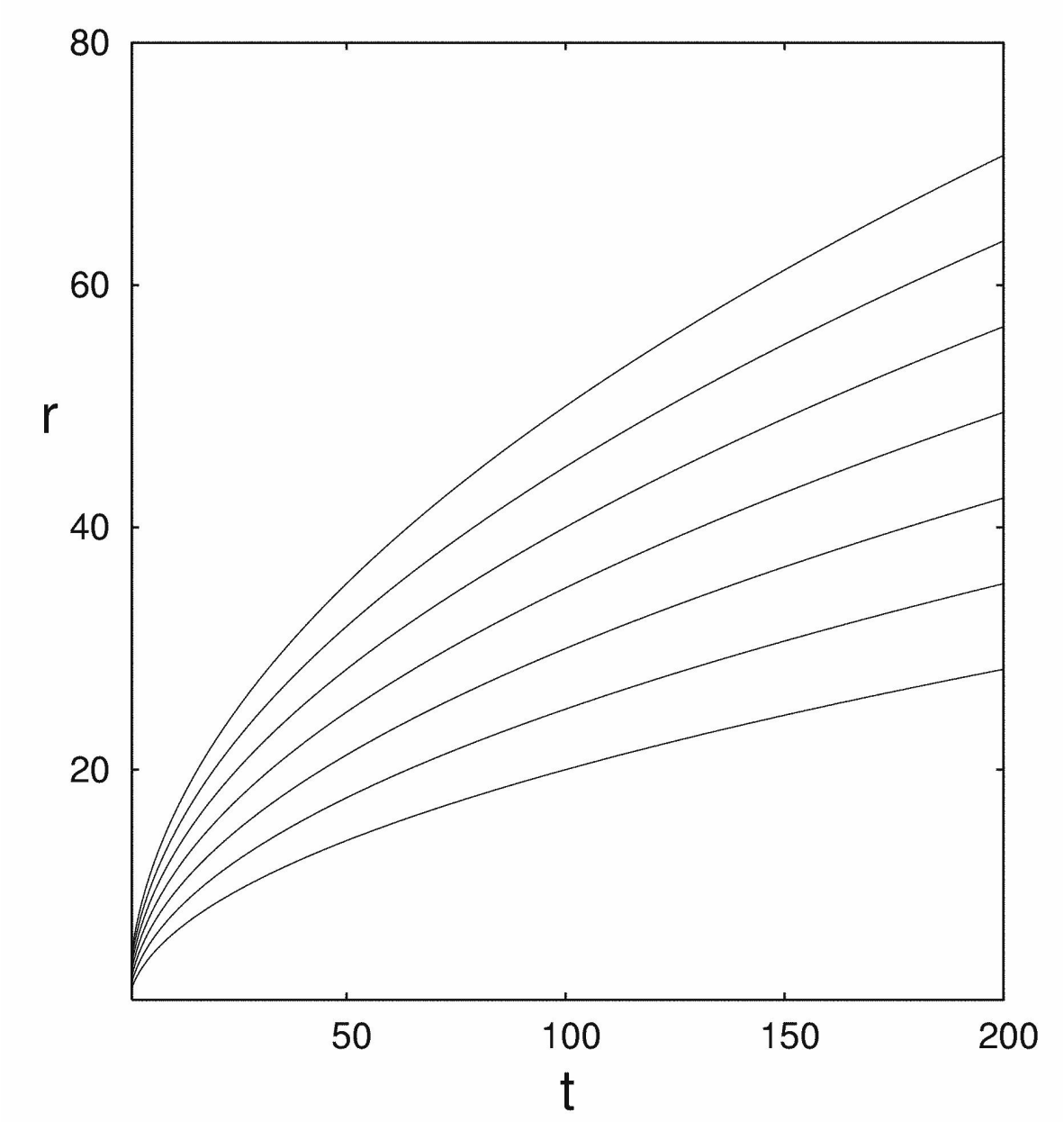


Figure 8 Phase function contours for the secondary wavefront in $n = 2$ dimensions, as described in Eq. (3.58) for immortal agent ($\gamma = 0$).

The inclusion of the non-linear mass balance term $\eta SA$ in Eq. (4.4) increases the rate of decay of infectious agent. The results of Sections 3.5 and 3.6 only hold if both $\gamma = 0$ and $\eta = 0$. The results of Section 3.4 are approximately true for sufficiently small $\eta$ and $A_0$. Otherwise, $\eta > 0$ only appears to introduce quantitative changes in the dynamics. In the special case of $D_S = D_I = \rho = 0$, the arguments of Section 3.3 can be extended to obtain the asymptotic approximation

$$c^* = \frac{S_0 - 1}{\sqrt{\gamma + \eta S_0 + S_0 - 1}}, \tag{4.5}$$

which agrees with Eq. (3.23) when $\eta = 0$.

In the limit of strong mixing, where spatial effects can be neglected, Eqs. (4.1)-(4.4) have a unique one-parameter family of asymptotically stable steady-states $(S, I, R, A) = (u, 0, S_0 - u, 0)$, where $u$ is determined by the initial conditions. In the presence of weak mixing, as long as $D_S > 0$, the asymptotic equilibrium will also be a spatially uniform distribution of this form.

Invasion speed approximations can be made based on the assumption that the minimum invasion speed of the linearized model corresponds to the actual invasion speed of the non-linear model. This assumption is sometimes referred to as the "linear conjecture" (Weinberger et al., 2002; Mollison, 1991). Potential candidates for the asymptotic invasion speed $c$ will be solutions of the eigenvalue problem

$$\det\left(\left\{s^{-1}M + sD - cI\right\}\right) = 0 \tag{4.6}$$

corresponding to non-negative eigenvectors, where

$$M = \begin{bmatrix} 0 & S_0 & S_0 \\ 0 & S_0 - 1 & S_0 \\ 0 & \rho & -(\eta S_0 + \gamma) \end{bmatrix}, \quad \text{and} \quad D = \begin{bmatrix} D_S & 0 & 0 \\ 0 & D_I & 0 \\ 0 & 0 & 1 \end{bmatrix}. \tag{4.7}$$

In linear conjecture invasion problems, $c^*$ is found by minimizing the appropriate eigenvalue over all positive $s$. When this computation was performed, I found reasonable agreement between the observed speeds and the asymptotically speeds predicted by linearization (see Fig. 9). Recently, Weinberger et al. (2002) have proven that the linear conjecture is true

for a class of cooperative systems with dispersal. However, the term "conjecture" remains appropriate for our problem because the linearized system $M$ fails to satisfy conditions ii. and v. of Hypothesis 4.1 of their theorem (Weinberger et al., 2002). A detailed analysis of the invasion speed problem for the extended SIR-A model will not be undertaken here. I will only make a few preliminary observations.

The characteristic polynomial of Eq. (4.6) is cubic equation in $c(s)$, implying a potential for three roots. One of these roots corresponds to a wave of purely susceptible individuals, and is not of immediate interest in the context of the SIR-A model. Of the two remaining speeds, one speed ($c_I^*$) roughly corresponds with a wave that is primarily driven by the dispersal of infectious individuals, and the other speed ($c_A^*$) roughly corresponds with a wave that is primarily driven by the dispersal of infectious agent. If there is no virus shedding ($\rho = 0$), these two speeds can be constructed explicitly. $c_I^*$ is the same as the rabies speed calculated by Kallen et al., shown in Eq. (1.3), and

$$c_A^* = \frac{S_0 - 1 + D_I(\gamma + \eta S_0)}{\sqrt{(1 - D_I)(\gamma + \eta S_0 + S_0 - 1)}}. \tag{4.8}$$

Note that these speeds are obtained through analysis of the characteristic polynomial, and without resort to the Laplace method in Section 3.3. Which of the two waves dominates dispersal appears to depend upon the dispersal rate of infectious individuals $D_I$. If

$$D_I < \frac{S_0 - 1}{\gamma + \eta + (\eta + 2)(S_0 - 1)}, \tag{4.9}$$

then $c_A^* > c_I^*$, and the invasion front is primarily driven by the dispersal of the infectious agent. Otherwise, the invasion front is primarily driven by the dispersal of infectious individuals, and $c_A^*$ loses physically significance.

As noted in Section 3.3, the invasion front associated with $c_A^*$ is probably unstable in the absence of infectious agent production ($\rho = 0$). However, numerical solution of the eigenvalue problem and regular perturbation analysis suggest that $c_A^*$ is a lower bound and reasonable zeroth-order approximation in the presence of virus shedding ($\rho > 0$). In the absence of

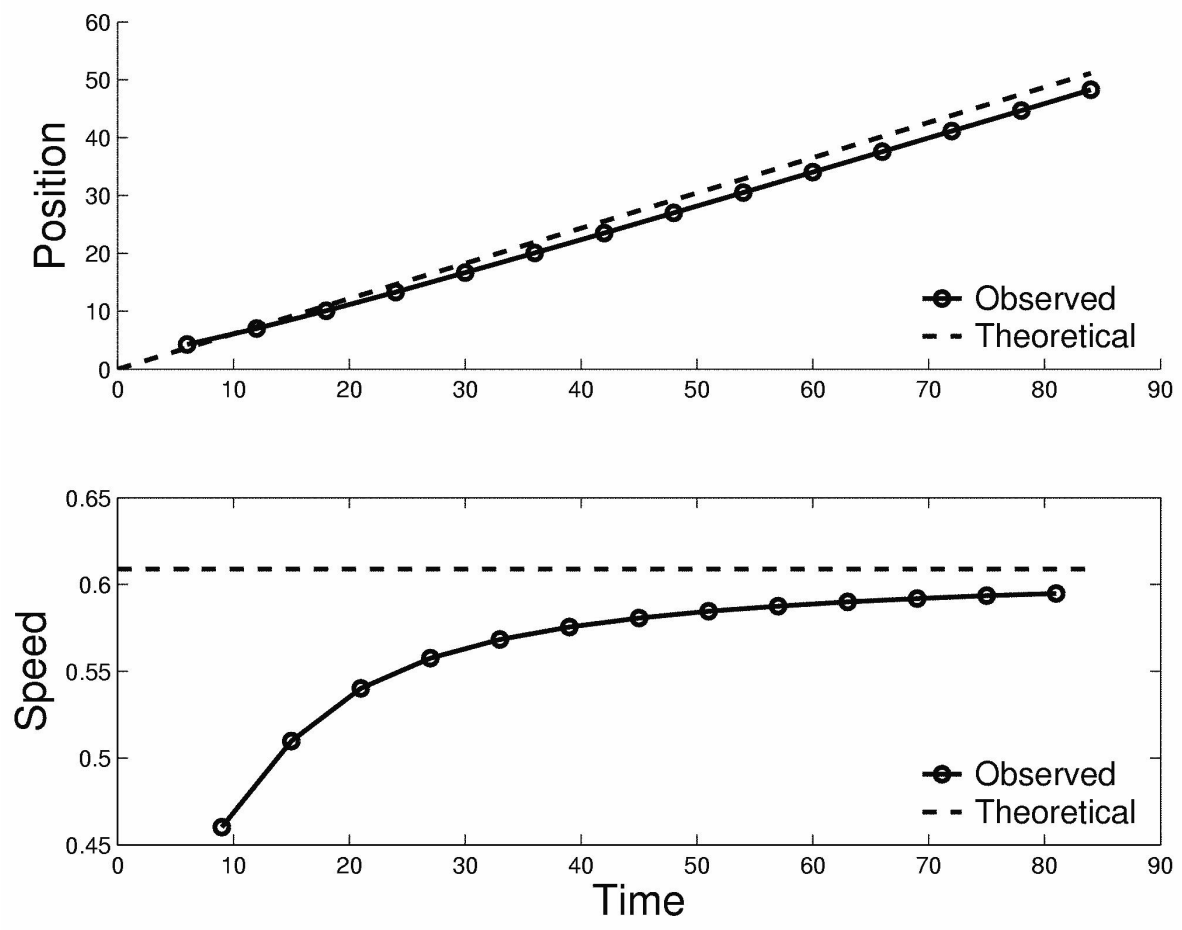


Figure 9 Plots of the position (top) and approximate instantaneous speeds as measured at an $S = 1$ threshold, with the parameters from Fig. 6. The observed speed appears to converge to the theoretical linear speed approximation, numerically calculated from the eigenvalue problem, Eq. (4.6), as $c_A^* \approx 0.6088$.

population dispersal ($D_S = D_I = 0$), a low order perturbation corrections to $c_A^*$, for $\rho > 0$, is

$$c_A^* = \frac{S_0 - 1}{\sqrt{\gamma + \eta S_0 + S_0 - 1}} + \sqrt{\frac{\rho S_0 (S_0 - 1)(S_0 + 2\eta S_0 + 2\gamma - 1)}{(\gamma + \eta S_0 + S_0 - 1)^3}} + o(\rho^{1/2}). \tag{4.10}$$

In the case of $\eta = \rho = 0$, we again obtain Eq. (3.23). Thus, the result of Section 3.3 appears to provide an important lower bound on the invasion rate in the presence of virus shedding.

# 5 Discussion

In this paper, I have presented the SIR-A equations (2.1)-(2.6) as a simple pedagogical model for the spatial dynamics of an epidemic following the point release of an infectious agent. By combining the separate pieces of mathematical analysis in Section 3, we can obtain a good picture of the epidemic's dynamic history. If the infectious agent is sufficiently potent for the given population concentration ( $S_0 = \hat{S}_0 \hat{\beta}_I / \hat{\mu} > 1$ ), the primary phase of the epidemic will sweep through the population in the form of a wavefront with asymptotic speed (in dimensional form)

$$\hat{c}^* = \frac{\left( \hat{S}_0 \hat{\beta}_I - \hat{\mu} \right) \sqrt{\hat{D}}}{\sqrt{\hat{\gamma} + \hat{S}_0 \hat{\beta}_I - \hat{\mu}}}, \tag{5.1}$$

and will reduce the susceptible population to a level below the critical threshold $\hat{\mu}/\hat{\beta}_I$. After the wavefront of the primary phase has passed, environmental exposure to persistent agent will continue to cause infection of susceptible individuals. This comprises a secondary phase of infection absent from standard models. The total amount of infection in this secondary epidemic phase will be proportional to the environmental half-life ($1/\hat{\gamma}$) of the agent. In the two dimensional case where the agent is immortal, the secondary phase will spread indefinitely, occupying an area roughly proportional to the time since release. In the case of insufficient population density, ($S_0 = \hat{S}_0 \hat{\beta}_I / \hat{\mu} < 1$), the primary phase will be absent, but the secondary phase will still be observable.

When the SIR-A model is extended by incorporating mass balance, dispersal of individuals, and virus shedding (Eqs. (2.7)-(2.10)) , the qualitative features of the SIR-A model

persisted under the various appropriate limits. Specifically, we can observe a primary phase of epidemic with constant asymptotic speed, followed by a slower secondary phase. Calculation of the speed of the primary phase wave front is more complex in the extended SIR-A model, but numerical solution of the linear conjecture appears to provide a reasonable approximation in cases where individual dispersal is slow relative to agent dispersal and virus shedding is small. The linear conjecture also provides a second method for derivation of Eq. (3.23) in the appropriate limits. Other potentially important extensions associated with many diseases but not incorporated here are latent stage classes and time delays.

The analysis of the SIR-A model is of mathematical interest because of its novelty and tractability. Other than the recently published work of Cook (Murray, 2003), the theoretical epidemiology literature apparently contains few examples where spatial dynamics have been reinterpreted as a spatio-temporal forcing of local dynamics. Because the model can be reduced to a system of ordinary differential equations, many standard methods can be used in the analysis. As a consequence, we can obtain a very complete picture of the dynamic behavior analytically. The presence of two distinct wave phenomena, both driven by diffusion does not seem to have been previously observed in such a simple model. Although the mathematical analysis for initial conditions other than a point release will be more complex, the linearity of Eq. (2.6) implies that any compactly supported initial condition for agent release should have similar asymptotic behavior.

The SIR-A model has some interesting implications for the general theory of waves in reaction–diffusion equations. Of central concern is the failure of Eq. (3.23) to correctly describe the speed of invasion when extended to a stochastic setting. Future work may better illuminate the relationships between stochastic invasions, and their deterministic counterparts. In addition, the qualitative distinctions between pushed and pulled waves (Lewis and Kareiva, 1993) are confused by the SIR-A model. Since both susceptible and infectious individuals are stationary, the resulting waves can not be classified as being pushed or pulled by reaction effects, but a fixed-speed wave is still observed. Further analysis, including stability analysis with respect to deterministic and stochastic perturbations and a careful treatment of

the extended SIR-A model, may provide some enlightenment.

## Acknowledgments

I would like to thank Jan Medlock for the inspirational discussions that lead to this work. I also thank Rafael Meza, Mark Kot, and one anonymous reviewer for their helpful comments on this manuscript. This work was supported by NSF VIGRE grant DMS-9810726.

## References

Abramowitz, M., Stegun, I., 1972. Handbook of Mathematical Functions with Formulas, Graphs, and Mathematical Tables, 10th Edition. National Bureau of Standards, Washington, D.C.

Acheson, D. J., 1990. Elementary Fluid Dynamics. Oxford University Press, New York, NY.

Bailey, N. T. J., 1975. The Mathematical Theory of Infectious Diseases, 2nd Edition. Griffin, London, UK.

Bluman, G. W., Anco, S. C., 2002. Symmetry and integration methods for differential equations. Springer, New York, NY.

Breman, J. G., Henderson, D. A., April 2002. Current concepts - diagnosis and management of smallpox. New England Journal of Medicine 346 (17), 1300–1308.

Caraco, T., Glavanakov, S., Chen, G., Flaherty, J. E., Ohsumi, T. K., Szymanski, B. K., September 2002. Stage-structured infection transmission and a spatial epidemic: A model for lyme disease. American Naturalist 160 (3), 348–359.

Clark, J. S., Lewis, M., Horvath, L., 2001. Invasion by extremes: population spread with variation in dispersal and reproduction. American Naturalist 152, 204–224.

Corless, R. M., Gonnet, G. H., Hare, D. E. G., Jeffrey, D. J., Knuth, D. E., 1996. On the Lambert W function. Advances in Computational Mathematics 5, 329–359.

Erdelyi, A., 1956. Asymptotic Expansions. Dover Publications, New York, NY.

Fauci, A. S., February 20 2003. Biodefense on the research agenda. Nature 142, 787.

Gradshteyn, I. S., Ryzhik, I. M., Jeffrey, A., 1980. Table of Integrals, Series, and Products. Academic Press, New York, NY.

Grindrod, P., 1996. The Theory and Applications of Reaction–Diffusion Equations: Patterns and Waves, 2nd Edition. Clarendon Press, Oxford, UK.

Henderson, D. A., February 26 1999. The looming threat of bioterrorism. Science 283, 1279–1282.

Henson, S. M., Constantino, R. F., Cushing, J. M., Desharnais, R. A., Dennis, B., King, A. A., October 19 2001. Lattice effects observed in chaotic dynamics of experimental populations. Science 294.

Kallen, A., Arcuri, P., Murray, J. D., 1985. A simple model for the spatial spread and control of rabies. Journal of Theoretical Biology 116, 377–394.

Kendall, D., 1965. Mathematical models of the spread of infection. In: Mathematics and Computer Science in Biology and Medicine. H. M. Stationary Office, London, pp. 213–225.

Kermack, W. O., McKendrick, A. G., 1991. Contributions to the mathematical-theory of epidemics .1. (reprinted from proceedings of the royal society, vol 115a, pg 700-721, 1927). Bulletin of Mathematical Biology 53 (1-2), 33–55.

Kevorkian, J., 1990. Partial Differential Equations: Analytic Solution Techniques. Chapman & Hall, London, UK.

Kevorkian, J., Cole, J. D., 1996. Multiple Scale and Singular Perturbation Methods. Springer, New York, NY.

Lewis, M. A., Kareiva, P., April 1993. Allee dynamics and the spread of invading organisms. Theoretical Population Biology 43 (2), 141–158.

Mollison, D., 1991. Dependence of epidemic and population velocities on basic parameters. Mathematical Biosciences 107, 255–287.

Murray, J. D., 2003. Mathematical Biology, 3rd Edition. Springer Verlag, New York, NY.

Noble, J. V., August 30 1974. Geographic and temporal development of plagues. Nature 250, 276–279.

Segal, L. A., Slemrod, M., September 1989. The quasi-steady-state assumption: A case study in perturbation. SIAM Review 31 (3), 446–477.

Snyder, R. E., 2003. How demographic stochasticity can slow biological invasions. Ecology 84, 1333–1339.

Weinberger, H. F., Lewis, M. A., Li, B., 2002. Analysis of the linear conjecture for spread in cooperative models. Journal of Mathematical Biology, 183–218.

# A Diffusion with Exponential Decay

In polar coordinates, the diffusion equation with exponential decay,

$$\frac{\partial u}{\partial t} = \frac{\partial^2 u}{\partial r^2} + \frac{n-1}{r}\frac{\partial u}{\partial r} - \gamma u \,, \tag{A.1}$$

has the fundamental solution

$$u(t,r) = (4\pi t)^{-n/2} e^{-\frac{r^2}{4t} - \gamma t} \,. \tag{A.2}$$

This can be proven using standard techniques from partial differential equations (Kevorkian, 1990). The maximum value of the solution $u(t,r)$ for a given radius $r$ occurs at

$$t_{max} = \frac{n}{4\gamma}\left(\sqrt{1+4\frac{\gamma r^2}{n^2}}-1\right) , \tag{A.3}$$

unless $\gamma = 0$, in which case,

$$t_{max} = \frac{r^2}{2n} . \tag{A.4}$$

For large $\gamma$ or $r$, the first order asymptotic approximation is

$$t_{max} \sim \frac{r}{\sqrt{4\gamma}} , \tag{A.5}$$

and the maximum value is exponentially small in $r$,

$$u(t_{max},r) \sim \left(\frac{\sqrt{\gamma}}{2\pi r}\right)^{n/2} e^{-r\sqrt{\gamma}} . \tag{A.6}$$

# B Properties of the Integrated Fundamental Solution

As is seen from the analysis of Section 3, many results for this model pivot on understanding the integral of the fundamental solution

$$\int_0^t A(t,r,\gamma,A_0)\,dt . \tag{B.1}$$

In some cases, like Eq. (3.16), the same integral arises with slightly different parameters. While I am unaware of a closed-form representation for Eq. (B.1), the asymptotic behavior of the integral is well known. In the limiting form of $t$ approaching infinity, (Gradshteyn et al., 1980),

$$\int_0^\infty A(t,r;\gamma,A_0)dt = A_0\int_0^\infty (4\pi t)^{-n/2} e^{-\frac{r^2}{4t}-\gamma t}dt \tag{B.2}$$

$$= \frac{A_0 r}{\sqrt{\gamma}}\left(\frac{\sqrt{\gamma}}{2\pi r}\right)^{n/2} K_{1-n/2}(r\sqrt{\gamma}), \tag{B.3}$$

where the modified Bessel functions $K_\nu(x)$ have algebraic singularities of order $x^{-\nu}$ for small inputs and decrease monotonically to zero, decaying exponentially for large inputs (Abramowitz and Stegun, 1972). For common $n$, Eq. (B.3) can be simplified. If $n = 1$,

$$\int_0^\infty A(t,r;\gamma,A_0)dt = \frac{A_0}{2\sqrt{\gamma}}\, e^{-r\sqrt{\gamma}}\,. \tag{B.4}$$

If $n = 2$,

$$\int_0^\infty A(t,r;\gamma,A_0)dt = \frac{A_0}{2\pi} K_0\left(r\sqrt{\gamma}\right)\,. \tag{B.5}$$

If $n = 3$,

$$\int_0^\infty A(t,r;\gamma,A_0)dt = \frac{A_0}{4\pi r}\, e^{-r\sqrt{\gamma}}\,. \tag{B.6}$$

If $\gamma = 0$ the modified Bessel function representation of Eq. (B.2) is singular, but the common cases can be handled individually. When $\gamma = 0$ and $n > 2$,

$$\int_0^\infty A(t,r;0,A_0)dt = \frac{A_0 r^{2-n}}{4\pi^{n/2}}\Gamma\left(\frac{n-2}{2}\right)\,, \tag{B.7}$$

where $\Gamma(x)$ is the gamma function (Abramowitz and Stegun, 1972). In the special case of $n = 3$, Eq. (B.7) reduces to

$$\frac{1}{4\pi r}\,. \tag{B.8}$$

If $\gamma = 0$ and $n \leq 2$, Eq. (B.2) can not be represented by the gamma function, and is in fact divergent. In these cases, the interesting property is the divergence rate of Eq. (B.1) as a function of the upper limit $t$. When $n = 1$,

$$\int_0^t (4\pi\tau)^{-1/2} e^{-\frac{r^2}{4\tau}} d\tau = \sqrt{\frac{t}{\pi}} e^{-\frac{r^2}{4t}} - \frac{r}{2}\,\mathrm{erfc}\left(\frac{r}{2\sqrt{t}}\right)\,, \tag{B.9}$$

where $\mathrm{erfc}(x)$ is the complementary error function (Abramowitz and Stegun, 1972). By inspection, we see that the divergence is on the order of $\sqrt{t}$ for fixed $r$. When $n = 2$,

$$\int_0^t (4\pi\tau)^{-1} e^{-\frac{r^2}{4\tau}} d\tau = \frac{1}{4\pi}\int_{\frac{r^2}{4t}}^\infty \frac{1}{u} e^{-u} du = \frac{1}{4\pi}\mathrm{E}_1\left(\frac{r^2}{4t}\right)\,, \tag{B.10}$$

where $\mathrm{E}_1(x)$ is the exponential integral of type 1 (Abramowitz and Stegun, 1972). Standard series expansions show that the integral diverges logarithmically in $t$ for fixed $r$.